Evidence for a rapid release of carbon at the Paleocene-Eocene thermal maximum

James D. Wright[a,1] and Morgan F. Schaller[a,b]

[a]Department of Earth and Planetary Sciences, Rutgers University, Piscataway, NJ 08854; and [b]Department of Geological Sciences, Brown University, Providence, RI 02912

Edited* by Wallace S. Broecker, Columbia University, Palisades, NY, and approved August 5, 2013 (received for review May 14, 2013)

The Paleocene/Eocene thermal maximum (PETM) and associated carbon isotope excursion (CIE) are often touted as the best geologic analog for the current anthropogenic rise in pCO_2. However, a causal mechanism for the PETM CIE remains unidentified because of large uncertainties in the duration of the CIE's onset. Here, we report on a sequence of rhythmic sedimentary couplets comprising the Paleocene/Eocene Marlboro Clay (Salisbury Embayment). These couplets have corresponding $\delta^{18}O$ cycles that imply a climatic origin. Seasonal insolation is the only regular climate cycle that can plausibly account for $\delta^{18}O$ amplitudes and layer counts. High-resolution stable isotope records show 3.5‰ $\delta^{13}C$ decrease over 13 couplets defining the CIE onset, which requires a large, instantaneous release of ^{13}C-depleted carbon. During the CIE, a clear $\delta^{13}C$ gradient developed on the shelf with the largest excursions in shallowest waters, indicating atmospheric $\delta^{13}C$ decreased by ∼20‰. Our observations and revised release rate are consistent with an atmospheric perturbation of 3,000-gigatons of carbon (GtC).

carbon cycle | climate change

Deep sea carbon isotope and $CaCO_3$ records across the Paleocene/Eocene thermal maximum (PETM) and associated carbon isotope excursion (CIE) (55.8 Mya) require a massive addition of ^{13}C-depleted carbon to the ocean–atmosphere system in a geologically short interval of time (1–3). Proposed mechanisms include the destabilization of the global methane reservoir by a thermal trigger (2, 4) or physical disturbance (5), production of thermogenic CH_4 and CO_2 during the emplacement of a large igneous province (6, 7), wildfires burning peatlands (8), desiccation of a large epicontinental sea (9), decomposition of terrestrial permafrost (10), and bolide impact (11, 12). The only consensus is that a precise chronology providing rates for the onset of the CIE is essential to distinguish among these mechanisms. Efforts to establish such a chronology have relied on average sedimentation rates based on integrated magneto- and biostratigraphic constraints (1), identifying cycles in deep sea cores and assigning an orbital periodicity (13, 14), or measuring the concentration of extraterrestrial ^{3}He and applying an estimated flux to establish sedimentation rates (15, 16). The lack of a precise timescale for the $\delta^{13}C$ excursion precludes further advances in identification of the source(s) of the light carbon and calculation of the release rates and magnitudes. Until these are better quantified, the relevance of the CIE as an analog for the Anthropocene remains speculative.

Deep sea bulk carbonate records show that the CIE began with an abrupt initial $\delta^{13}C$ decrease of ∼1‰ followed by a more gradual decrease of similar magnitude (17). Bulk carbonate $\delta^{13}C$ values from Ocean Drilling Program (ODP) Site 690 record the initial decrease in adjacent 1-cm samples. The cyclostratigraphic age model for Site 690 of Röhl et al. (13) constrains this initial decrease to <750 y, whereas the ^{3}He method of Murphy et al. (16) places the duration of this initial decrease at closer to 30 kya. Herein lies the chronologic conundrum: the 750-y and 30 kya durations of the initial excursion are based on the same deep sea $\delta^{13}C$ record and are essentially indistinguishable given the error in each methodology, yet have drastically different implications for the size of the carbon release necessary to produce the CIE. This uncertainty highlights the dire need for a precise chronometer for the onset of the carbon isotope excursion.

Here, we present high-resolution bulk stable isotope and % $CaCO_3$ records from the northern Salisbury Embayment [35°N paleolatitude (18)] on the Atlantic coastal plain, using the Millville (ODP 174X) and newly recovered Wilson Lake B cores. Both of these cores contain the upper Paleocene-lower Eocene Marlboro Clay unit that has been correlated to deep sea CIE sections using carbon isotope and biostratigraphy (19, 20). These cores have two unique features that distinguish them as outstanding temporal archives for the onset of the CIE: (*i*) expanded sections of the Marlboro Clay in both the Wilson Lake B (15.5 m) and Millville (12.6 m) cores and (*ii*) distinct and rhythmic bedding of silty clays through the entire section containing the $\delta^{13}C$ excursion.

The $\delta^{13}C$ excursions in the Wilson Lake B and Millville cores have amplitudes of −6‰ and −4.5‰, respectively (Fig. S1), with ∼3.5‰ of the decrease representing the virtually instantaneous initial $\delta^{13}C$ decrease observed in deep sea records (13, 17). In Wilson Lake B, this initial step in the $\delta^{13}C$ decrease is recorded from 112.29 to 111.00 m, whereas the same decrease is found between 273.85 and 273.39 m in the Millville core. In contrast, the correlative $\delta^{13}C$ decrease occurs over 1 cm at ODP Site 690 (13, 17). Therefore, our shallow marine records provide at least 45–130 times the temporal resolution afforded by the deep ocean record.

In the Wilson Lake B and Millville cores, the Marlboro Clay is characterized by rhythmic couplets of silty, kaolinitic clay (21, 22) distinguished by 1- to 2-mm layers of swelling smectite clays and micaceous silts, recurring every 1–3 cm through the entirety of the unit (mean, 1.9 ± 0.8 cm at 1σ) (Fig. 1). Harris et al. (19) noted similar layering in the Marlboro Clay interval in the Ancora core (ODP Leg 174X). The distinct layered beds are found in stratigraphically equivalent exposures in Medford, NJ, and in the South Dover Bridge core from Maryland (23). The prevalence and similarity of these couplets in at least five locations demonstrates that they are primary depositional features in the Marlboro Clay of the Salisbury Embayment. If these sedimentary cycles are demonstrably periodic, such layering offers the possibility of assigning a precise chronology to the onset of the CIE.

Significance

Calcium carbonate and carbon isotope records from the rhythmically bedded Marlboro Clay, deposited during the onset of the PETM CIE, show that the massive release of isotopically light carbon was instantaneous, providing important constraints for the magnitude of carbon released and potential mechanisms.

Author contributions: J.D.W. and M.F.S. designed research, performed research, analyzed data, and wrote the paper.

The authors declare no conflict of interest.

*This Direct Submission article had a prearranged editor.

[1]To whom correspondence should be addressed. E-mail: jdwright@rci.rutgers.edu.

This article contains supporting information online at www.pnas.org/lookup/suppl/doi:10.1073/pnas.1309188110/-/DCSupplemental.

Fig. 1. Examples of the remarkably cyclic sedimentary layering found throughout the Marlboro Clay in the Wilson Lake (*A* and *B*) and Millville (*C*) cores. (*A*) Core photograph of freshly split core from Wilson Lake B from 105.45 to 106.06 m (346–348 ft), ~2-cm-scale swelling clay couplets. (*B*) Same interval after desiccation. Original swelling clays now appear as dark banding. (*C*) Whole round section of the Millville core (IODP 174AX) from 262.13 to 263.96 m (860–866 ft, white cards) showing the same cyclic clay couplets. Photo taken shortly after recovery, core was scraped but not split; however, the couplets are still visible.

Temporal Origin of the Couplets Within the Marlboro Clay

The remarkably rhythmic layers are the most prominent feature of the Marlboro Clay on first visual inspection of the freshly split Wilson Lake B cores (Fig. 1). Recognizing the potential for a climatic control, we selected two intervals from the Wilson Lake B core for high-resolution sampling (2 mm): the first from 111.313 to 111.542 m spans 15 layers, recording deposition just after the initial $\delta^{13}C$ excursion (Fig. 2). A second transect between 107.936 and 108.036 m, spanning nine layers within the interval of low $\delta^{13}C$ values that characterize the high-frequency signal at the height of the CIE (Fig. S2; *SI Text*). The high-resolution $\delta^{18}O$ records from both segments covary with the physical expression of the layers, where each of the clay couplets corresponds to a single cycle in $\delta^{18}O$. Amplitudes of the $\delta^{18}O$ cycles have a mean of 1.1 ± 0.5‰, including two cycles between 111.313 and 111.351 m that have amplitudes of 2‰.

The variability in $\delta^{18}O$ reflects changes in temperature, the $\delta^{18}O$ of water ($\delta^{18}O_{water}$), or a combination of both. If ascribed solely to temperature, the 1.1 ± 0.5‰ range in $\delta^{18}O$ indicates oscillations of 4.8 ± 2.2 °C (24). If the $\delta^{18}O$ of bulk carbonate ($\delta^{18}O_{cc}$) was driven only by variations in $\delta^{18}O_{water}$ resulting from changes in fresh water flux, the $\delta^{18}O$ cycles indicate a range of 7.8 ± 3.6 practical salinity units (psu) in salinity [using a freshwater end-member $\delta^{18}O$ of −5 ± 1‰ from the modern Carolinas (25) and mixing over a salinity range of 35 psu (Figs. S3 and S4; *SI Text*)]. We maintain that temperature must be a significant component of the intracouplet $\delta^{18}O$ variability, especially for couplets that record 2‰ cycles; the required changes in salinity are far greater than are observed on the modern mid-Atlantic shelf (26, 27) or even at sites at comparable water depths off the Amazon fan (28). If half of the amplitude of the largest cycles were due to freshwater, the responsible process must be capable of producing cyclic temperature variations of ~4.5 °C, affecting the entire shelf surface–water system.

The clay couplets in the Millville core are strikingly similar in character to those observed in Wilson Lake B and show $\delta^{18}O$ cycles associated with each (Fig. 1). We count ~750 couplets at Millville, beginning just before the initial $\delta^{13}C$ decrease and continuing to the top of the unit, where the Marlboro is truncated by an erosional surface (total of 12.5 m). Presumably, this rhythmic bedding can be related to some cyclic depositional process, and given the tight association with periodic changes in $\delta^{18}O$, the most likely driver is something inherent to the climate system (29). Aside from tidal forcing of cyclic sedimentary packages, the dominant forcing within the climate system is related to changes in insolation. On depositional timescales, long period changes in Earth's orbital parameters have the greatest influence on insolation: those of eccentricity (95–125 and 413 kya), obliquity (41 kya), and precession (19 and 23 kya).

For the sake of discussion, if we consider a scenario where the layers are related to the ~20-kya precession of the equinoxes, where each clay couplet comprises a single cycle, the entirety of the unit would represent ~15 My of deposition (750 layers at 20 kya/layer). This extreme duration is not supported by biostratigraphic constraints through the interval (23, 30), and more importantly, the sediments of the Marlboro Clay have reversed magnetizations (11) and were deposited entirely during magnetochron C24r, precluding an ~15-My duration. Below the ~20-kya band, but above the seasonal cycle, there is no cyclic change in radiative forcing due to changes in earth's orbital parameters; a phenomenon referred to as the "orbital gap" by Munk et al. (31). A suite of periods and interfering harmonics within the millennial band have been suggested (32, 33), including a 1,500-y cycle observed in the North Atlantic that is purportedly orbitally driven (32). Even if each couplet was a single 1,500-y cycle, the Marlboro Clay sequence would represent about ~1.13 My of deposition, which is not supported by any bio- or cyclo-stratigraphic evidence (13, 19, 34). More importantly, the expected radiative forcing due to these millennial-scale (or shorter, e.g., sunspot) cycles is only on the order of a few watts per meter squared (35, 36), and hence, these mechanisms lack the requisite insolation forcing to result in the observed $\delta^{18}O$ changes reported here.

The next cycle of any substantial radiative consequence below orbital precession is due to seasonality (particularly at mid- and

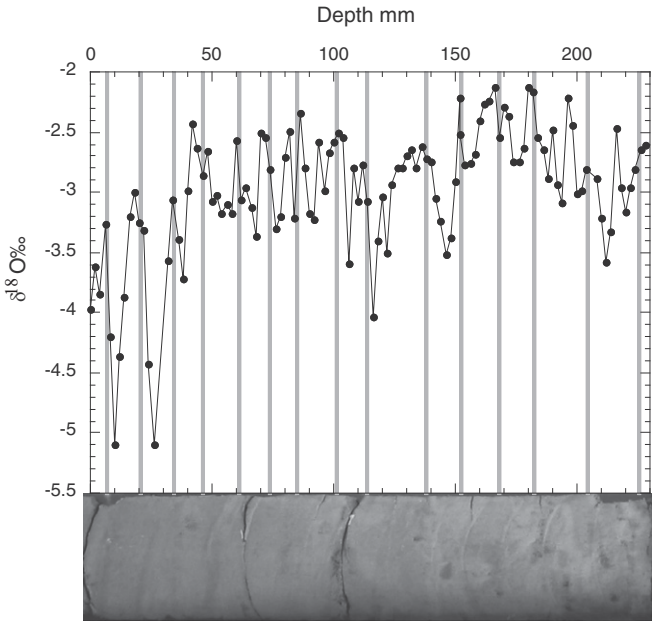

Fig. 2. Bulk $\delta^{18}O$ record from Wilson Lake B core with the starting depth of 111.313 m (365.2 ft) in the core. Samples were taken every 2 mm. Gray bars show the position of the lamina relative to stable isotope samples. The sample transect was taken down the middle of the core. The core photo is below. The couplet tops are defined as the occurrence of swelling smectite clays and correspond to increasing or maxima in $\delta^{18}O$ values.

high latitudes). At 35°N, the inferred paleo-latitude for the Millville and Wilson Lake locations (18, 20), annual insolation varies from ~200 to 500 Wm^{-2} (37) (far exceeding that of anything in the millennial band by several orders or even that of the precession cycle). A simple heat flux calculation indicates that a 300-Wm^{-2} variation would impart a 6 °C seasonal temperature cycle on the shelf (38). We use the Levitus and Boyer (39) gridded monthly data to estimate the contributions of temperature and $\delta^{18}O_{water}$ on calcite precipitated on the modern Carolina shelf and predict a seasonal range in $\delta^{18}O_{calcite}$ of 1.2 ± 0.2‰ for shelf locations at 50-m water depth at ~35°N (Fig. S4; *SI Text*). We note that oscillations in oxygen isotopes driven by seasonal temperature and/or fresh water flux variations in modern shelf settings are observed in shell transects of bivalves (40–42) and planktonic foraminifera from sediment traps (43, 44). The $\delta^{18}O$ cycles accompanying the layering observed in the Marlboro Clay are wholly consistent with seasonal changes forced by insolation at midlatitude sites.

The inference of seasonally paced deposition requires sedimentation rates on the order of 2 cm/y within the Salisbury Embayment. Mud accumulation rates in excess of 10 cm/y are observed on the modern Amazon shelf (45) and clays in the East China Sea (46), indicating that the high shelf sedimentation rate inferred from the Salisbury Embayment during the CIE cannot be excluded, especially under an enhanced hydrologic cycle (20). In fact, rapid accumulation of muds in ~50-m water depth for decades to centuries are common on shelves in regions with high suspended sediment load (45, 47). Therefore, we contend that the rhythmic bedding throughout the Marlboro Clay represents annual deposition, where each couplet corresponds to a seasonal cycle, resulting from highly turbid waters in the Salisbury Embayment (20).

Timing of the Onset of the CIE from High-Resolution Stable Isotopes in Millville

The Millville core was chosen for high-resolution study through the CIE because the $\delta^{13}C$ decrease (starting at 273.96 m) is wholly contained in the layered Marlboro Clay and therefore provides a chronometer through the CIE onset. We sampled the Millville core every 2 mm from the basal layer at 273.96–273.37 m, fully capturing the initial $\delta^{13}C$ decrease. Between 273.772 and 273.532 m, the $\delta^{13}C$ of bulk carbonate decreases by 3.9‰, from 1.45‰ to −2.48‰, over a span of 13 couplets (Fig. 3). This decrease is a maximum range because the −2.48‰ minimum value is part of a higher-frequency signal superimposed onto the near linear change of −3.5‰ over the 13 couplets. In contrast, $\%CaCO_3$ shows a more abrupt decrease, from 6% to 1% within one layer, with most of the change (4.25% to 1%) occurring across 4 mm (Fig. 3).

Bulk $\delta^{18}O$ decreases from −1.5‰ to −2.7‰ during the initial decrease in $\delta^{13}C$ (Fig. 3). As with $\delta^{13}C$, the $\delta^{18}O$ records higher-frequency cycles superimposed on this decreasing trend, which correspond to the depositional layers. We measured the thickness of each layer through the CIE recorded in Millville, using lightly polished slabs of the now dry core, and found a mean layer thickness through the interval of 19 ± 7 mm (SD). When the high-resolution $\delta^{18}O$ data from the CIE interval are filtered using this layer frequency, the tight correspondence (Fig. S5) indicates that the oscillations in $\delta^{18}O$ are reasonably described by the frequency of the sedimentary layers. Given that the oscillations in $\delta^{18}O$ have large amplitudes (0.73 ± 0.23‰), implying regular ≥3 °C changes in temperature, the cyclicity in $\delta^{18}O$ (and corresponding rhythmic bedding) are best explained by the seasonal insolation cycle. Therefore, we interpret the 13 observed layers through the onset of the CIE at Millville as 13 annual cycles, and the 750 layers within the Marlboro clay at Millville as representing 750 annual cycles.

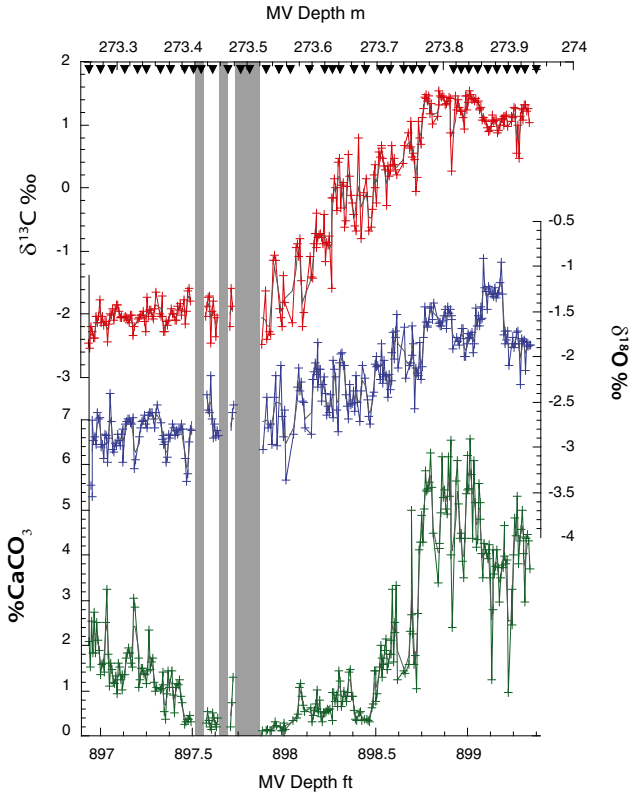

Fig. 3. High-resolution bulk stable isotope and percent carbonate data from the Millville core (IODP Leg 174AX) through the onset of the CIE. Depth scales are in meters (*Upper*) and feet (*Lower*; the drillers used 10-ft drill rods and feet units are preserved here to facilitate comparison with the original core descriptions). The $\delta^{13}C$ (red), $\delta^{18}O$ (blue), and $CaCO_3$ (green) records were generated by sampling the slabbed Millville cores at 2-mm intervals. Intervals with no data reflect too little or no $CaCO_3$ (<0.1%) are shown by the gray bars. The position of the clay couplets is denoted by the inverted triangles at top.

Surface Water $CO_{2(aq)}$ Concentrations and Carbon Isotopic Equilibrium

The interpretation of annual couplets makes a testable prediction: the response time of the surface water carbonate system should be much more rapid than the total equilibration time between the surface ocean carbon reservoir and the atmosphere. This difference should be reflected in the $\%CaCO_3$ and bulk $\delta^{13}C$ records from the shelf. Paleo-water depths are estimated (Fig. S6; *SI Text*) to be ~60 m at Millville at the start of the PETM; an atmospheric pCO_2 increase would propagate through the water column to this depth in a matter of weeks (48), increasing $[CO_2(aq)/H_2CO_3]$ enough to shift the carbonate equilibrium away from $CO_3^=$. In contrast, the $\delta^{13}C$ response depends on the rate of CO_2 exchange between the surface ocean and atmosphere (modern exchange is ~90 gigatons of carbon per year) (49), and radiocarbon measurements have been used to quantify this isotopic equilibration as occurring on the order of a decade (50, 51).

Our ability to resolve the differential response times in $\%CaCO_3$ (<1 couplet) and $\delta^{13}C$ (~13 couplets) at Millville (Fig. 3) requires a very high sedimentation rate. An annual forcing for the couplets matches the observed changes in the modern ocean with respect to the rates of CO_2 invasion (<1 y) and carbon isotopic equilibration (~1 decade). Therefore, the most parsimonious explanation for the difference in response times between $\%CaCO_3$ and $\delta^{13}C$ is a large and rapid injection of CO_2, supporting our interpretation that the couplets reflect annual depositional cycles. Any other interpretation for the origin of the

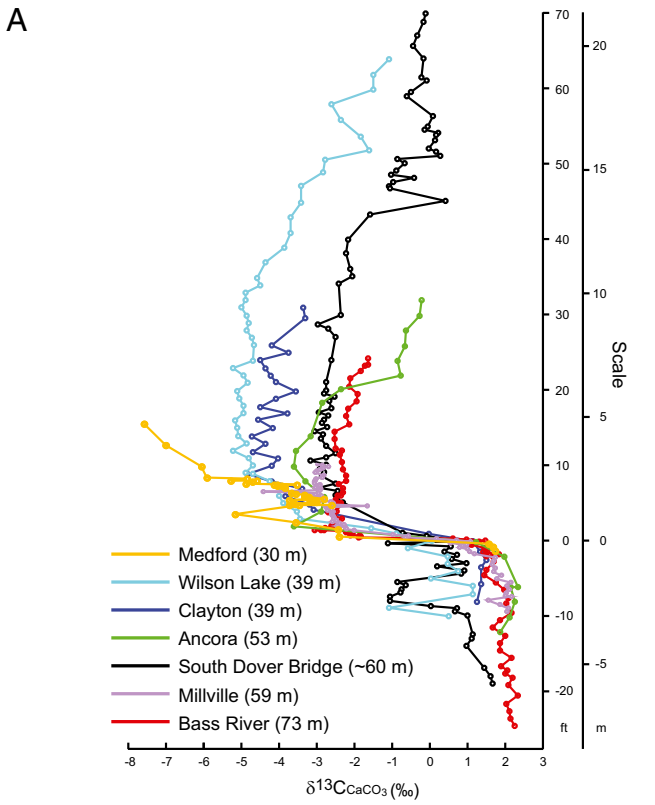

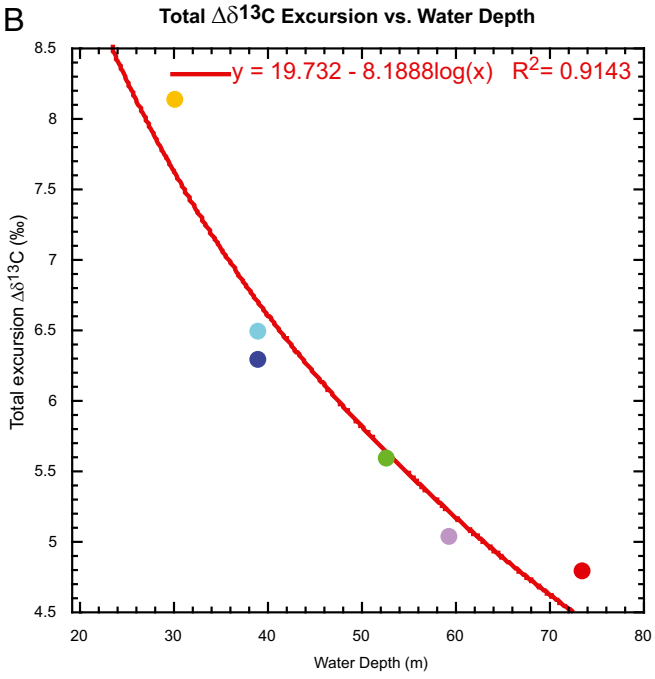

Fig. 4. (*A*) Comparison of the PETM carbon isotope excursion from several sites along a dip-transect from shallow to deep on the mid-Atlantic shelf (water depths calculated using simple projection onto a dip line with a slope of 1:1,000; *SI Text*). From deepest to shallowest: Bass River (red) (11), Ancora (green) (11), South Dover Bridge (black) (23), Clayton (dk. blue)(11), Wilson Lake B (lt. blue), Medford (orange; *SI Text*). Note the deepest sites show the smallest excursions, whereas the shallowest show the largest excursions, including the Medford locality, which is based on both outcrop and core. All Marlboro Clay sections are capped by an erosional unconformity. All Marlboro Clay sections are capped by an erosional unconformity. Depths in each core are recalculated with the initiation of the CIE defined as 0 m. (*B*) Relationship between total carbon isotope excursion *SI Text* and its paleo-water depth for each site along the dip transect. A logarithmic best fit (R^2 = 0.91) indicates that the very shallowest sites, those in unbuffered communication with the atmosphere, should show a total excursion of approximately −20‰ (*SI Text*). Data from the South Dover Bridge core not included due to large uncertainty in projection onto the dip transect.

couplets must account for the temporal responses of the carbonate chemistry and isotope change observed on the shelf during the PETM CIE. Invoking longer period forcing creates a conundrum, requiring as yet unspecified sources of carbon and additional feedbacks to explain these observations of the PETM CIE (52).

Reconciling the Marlboro Clay and Deep Ocean Chronologies

The rhythmic bedding within the Marlboro Clay implies a timescale for the onset of the CIE that on first inspection appears much different (by two to three orders of magnitude) than the chronology based on deep sea records (decades vs. 1–10 kya). We agree that published chronologies for the recovery interval derived from deep sea records are correct (e.g., cycle counting vs. ^{3}He). However, we argue that the anatomy of the CIE onset and its attendant chronology can only be obtained from recorders that are largely insulated from the open ocean, and the timescales being compared here are wholly compatible because (*i*) the Marlboro Clay records only the initiation of the CIE, <1000 y, and (*ii*) bulk $\delta^{13}C$ records from the open ocean are fatally imprinted by mixing/diffusion with older carbon from the deep ocean and have much lower sedimentation rates.

The $\delta^{13}C$ from the various Marlboro Clay sites indicate that most if not all Marlboro Clay sections do not record the recovery phase of the CIE documented in deep ocean sites. At the top of the Marlboro Clay, bulk $\delta^{13}C$ values remain −2.5‰ to −4.5‰ lower than preexcursion values (Fig. 4 *A* and *B*). On the contrary, deep ocean sites have $\delta^{13}C$ values that are <2.5‰ lower than preexcursion values at the start and <1‰ by the end of the recovery phase. The recovery phase of the CIE is well established as being on the order of 150 kya based on modeling (53–55), and these time scales have been validated by temporally well-constrained pCO_2 events associated with large igneous province emplacement (56, 57). A pCO_2 pulse introduced into the ocean–atmosphere system with an attendant $\delta^{13}C$ anomaly decays exponentially during the recovery phase, as modeled. If a CO_2 pulse is added directly to the atmosphere, the atmosphere and surface ocean (to a lesser extent) will initially experience much higher CO_2 concentrations and have a much larger $\delta^{13}C$ anomaly than the deep ocean. However, this initial change is both extremely rapid and transient, making it very difficult to observe without a high-resolution recorder that is in close communication with the atmosphere. Lack of this critical observation to date should not be construed as a flaw in our hypothesis; rather, a specific prediction that warrants significant further work (see below). After the CO_2 perturbation, the atmosphere and surface ocean will come into near equilibrium with the deep ocean on the 200- to 2,000-y scale (i.e., ∼70% of the initial pulse has dissipated) (58; Fig. S7) and then follow the well-constrained decay of the anomaly over ∼150 kya in the absence of additional perturbation, as predicted by geochemical modeling (53–55).

A CO_2 perturbation with ^{13}C-depleted carbon has different expressions in the atmosphere and surface ocean because of the mixing and diffusion with the deep ocean (*SI Text*). Measurements of surface ocean ^{14}C show that the CO_2 pool in those waters is a mix of modern atmosphere and much older CO_2 ventilated from the deep ocean (59). Bomb ^{14}C production during the 1950s and 1960s demonstrates that the timing and magnitude of a carbon isotope perturbation differs between the atmosphere, surface ocean, and deep ocean. The atmosphere

recorded a near instantaneous shift with a large $\Delta^{14}C$ response, whereas peak surface ocean invasion was about a decade later with an attenuated Δ ^{14}C signal (51). This response is nearly identical to our observations of the onset of the CIE at Millville: the precipitous drop in wt% $CaCO_3$ (evidence of a rapid increase in $[CO_2]_{aq}$), followed by a slower, decadal scale invasion of ^{13}C-depleted carbon to the surface water system (Fig. 3). Most of the modern deep ocean has yet to be influenced by bomb ^{14}C (Fig. S4). This modern experiment implies that the large (up to 8.2‰) $\delta^{13}C$ signal of the Marlboro Clay represents the initial phase of ocean invasion (<2,000 y). It also predicts that the atmospheric response was larger than the 7‰ $\delta^{13}C$ decrease observed in soil carbonates (60).

Aside from visual similarity, there is no other a priori reason to assign deep sea chronologies to shelf records (thereby forcing them to artificially conform to a recovery phase). In the case of the Salisbury Embayment, this miscorrelation is simply a function of our poor understanding on the exact timing of the erosional truncation at the top of the Marlboro Clay, within the overall global-scale context of the CIE. Therefore, our interpretation of the shelf sites containing the Marlboro Clay is that they do not preserve any of the later sediments that would comprise the recovery phase and hence do not record the time period of chemical and isotopic reequilibration of the surface ocean/atmosphere system with the deep ocean. This perspective effectively divorces the shelf chronologies from the deep ocean records as they pertain to the onset of the CIE. The $\delta^{13}C$ values in the Marlboro Clay are best interpreted as a record of the initial CO_2 perturbation to the atmosphere and its infiltration into the surface ocean. In fact, this interpretation is allowable by biostratigraphic data, which have 100- to 200-kya resolution at best (23). The apparent $\delta^{13}C$ recovery in the upper part of the Marlboro actually represents the transfer of CO_2 (with its anomalous $\delta^{13}C$ value) from the atmosphere/surface ocean reservoir into the deep ocean. Using our timescale, the ∼750-y timespan recorded is wholly consistent with the 200- to 2,000-y timescale of Archer et al.'s (58) synthesis of model predictions for the current anthropogenic increase. Thus, the shelf recovery is a separate event from the recovery observed in the deep ocean carbonate records, in both its root cause and its timescale, and comparison between the two is inappropriate and has led to significant miscorrelation (61–63).

Atmospheric Response to PETM CIE

A requirement of the near instantaneous release of ^{13}C-depleted CO_2 is a much larger excursion in the atmosphere than has been measured to date. We show $\delta^{13}C$ excursions of approximately −8.2‰ at the shallowest shelf sites (Medford, 30-m water depth) to −3.5‰ at the deepest (Bass River, ∼73 m; Fig. 4*A*). At the peak of the CIE, a clear $\delta^{13}C$ gradient had developed on the shelf, with the lowest values and largest excursions recorded at the shallowest sites (Medford) and the smallest excursions at the deepest sites (Bass River). When the total magnitude of each excursion is compared with paleo-water depth of the corresponding site, an unambiguous trend emerges that can be extrapolated to the origin, yielding an expected atmospheric perturbation of approximately −20‰ (Fig. 4*B*; *SI Text*). Because the magnitude of the $\delta^{13}C$ anomalies are a function of the extent to which mixing with the deep ocean overprints each record (as evidenced by modern bomb ^{14}C), we hypothesize that the total atmospheric excursion is much larger than the measured 8‰ excursion at Medford and has simply yet to be identified. Furthermore, as an atmospheric perturbation integrates over the successively larger and slower reacting reservoirs, the total magnitude of the excursion is attenuated; at the opposite extreme of the gradient, deep sea $\delta^{13}C$ excursions (based on benthic foraminiferal records) are −2.7 ‰ in the South Atlantic and Southern Ocean (1) and approximately −2‰ in the Indo-Pacific (64).

We note that some shelf sections have been used to argue for a more protracted release of carbon (14, 65). Most notably, Cui et al. (14) identified a $\delta^{13}C$ excursion of −4.5‰ in bulk organic matter from a section near Spitsbergen. The total excursion there is slightly less than predicted from our observations in the Salisbury Embayment (unless the site is at a paleo-water depth of ∼70 m; Fig. 4*B*), an effect that is probably related to the incorporation time and residence time of organic matter on the shelf, which is known to have a lag on the order of 1,000 y (66) and is differentially diachronous (67). More importantly, the slow release rate is a function of assigning precessional forcing to cyclicity in manganese and iron in constructing their timescale, in part based on the assumption of synchrony with the deep sea, which we argue above is inappropriate for the $\delta^{13}C$ onset in shelf localities.

Implications for the Rate of Carbon Release and Sequence of Events at the PETM

The single greatest hurdle hindering understanding of the PETM CIE has been uncertainty in the timing of the carbon added to the ocean–atmosphere system: the release schedule greatly affects the amount of ^{13}C-depleted carbon necessary to produce the globally observed CIE at any given isotope composition, due to the differential reaction time of Earth's exchangeable carbon reservoirs (68, 69). The second unknown has been the size of the atmospheric response. Our high-resolution stable isotope records from the Marlboro Clay provide constraints for both. We demonstrate that the initial release was rapid, if not instantaneous. A best fit of the relationship between the total CIE magnitude and paleo-water depth at each site (Fig. 4*B*) predicts an atmospheric excursion of −20‰ (R^2 = 0.91; *SI Text*). Assuming a pre-CIE atmospheric reservoir of 2,000 GtC (with a $\delta^{13}C$ of −6‰) (70) and an instantaneous release, a mass balance calculation gives an estimate of the amount of carbon necessary to produce the ∼20‰ atmospheric excursion. No realistic amount of organic carbon (approximately −26‰) can produce a −20‰ atmospheric change (>100,000 GtC is needed). Thermogenic (−40‰) and biogenic methane (−60‰) sources would require 2,900 and 1,200 GtC, respectively, to produce the −20‰ atmospheric excursion. Given the rapidity of the onset, magnitude of the $\delta^{13}C$ excursion, and that the observed calcite compensation depth shoaling in deep ocean requires ∼3,000 GtC (3), two mechanisms meet these criteria: large igneous province-produced thermogenic methane (6, 7) and cometary carbon (11, 12). The latter is consistent with the recent discovery of a substantial accumulation of nonbiogenic magnetic nanoparticles in the Marlboro clay, whose origin is best ascribed to impact condensate (71). If released as CO_2, this would be consistent with observations of an ∼5 °C global warming, although we note that the radiative effect of a methane release, while short lived, is substantially greater than CO_2. Finally, the revised timescale for the rate of carbon release at the onset of the PETM limits its usefulness as an analog for our current anthropogenic release.

ACKNOWLEDGMENTS. This work benefitted greatly from discussions with Ken Miller, who noted that other cores from the New Jersey coastal plain displayed layering in the Marlboro, which prompted us to look at the Millville core in detail. Dennis Kent and Robert Kopp provided valuable discussions. Richard Mortlock, Nicole Abdul, and Elizabeth Miller helped with sample preparation and stable isotope analyses. We thank Jeff Severinghaus and Gerald Haug who provided insightful reviews that greatly benefitted the final manuscript. We also acknowledge three anonymous reviewers who provided helpful reviews on an earlier version of the manuscript. This work was funded by National Science Foundation Grant 0958867.

1. Kennett JP, Stott LD (1991) Abrupt deep-sea warming, palaeoceanographic changes and benthic extinctions at the end of the Palaeocene. *Nature* 353(6341):225–229.
2. Dickens GR, O'Neil JR, Rea DK, Owen RM (1995) Dissociation of oceanic methane hydrate as a cause of the carbon isotope excursion at the end of the Paleocene. *Paleoceanography* 10(6):965–971.
3. Zachos JC, et al. (2005) Rapid acidification of the ocean during the Paleocene-Eocene thermal maximum. *Science* 308(5728):1611–1615.
4. Matsumoto R (1995) ^{13}C anomalies of carbonates and a new paradigm 'gas-hydrate hypothesis'. *J Geol Soc Jap* 101(11):902–924.
5. Katz ME, Cramer BS, Mountain GS, Katz S, Miller KG (2001) Uncorking the bottle: What triggered the Paleocene/Eocene thermal maximum methane release? *Paleoceanography* 16(6):549–562.
6. Svensen H, et al. (2004) Release of methane from a volcanic basin as a mechanism for initial Eocene global warming. *Nature* 429(6991):542–545.
7. Storey M, Duncan RA, Swisher CC, 3rd (2007) Paleocene-Eocene thermal maximum and the opening of the Northeast Atlantic. *Science* 316(5824):587–589.
8. Kurtz AC, Kump LR, Arthur MA, Zachos JC, Paytan A (2003) Early Cenozoic decoupling of the global carbon and sulfur cycles. *Paleoceanography* 18(4):1090.
9. Higgins JA, Schrag DP (2006) Beyond methane: Towards a theory for the Paleocene-Eocene Thermal Maximum. *Earth Planet Sci Lett* 245(3–4):523–537.
10. DeConto RM, et al. (2012) Past extreme warming events linked to massive carbon release from thawing permafrost. *Nature* 484(7392):87–91.
11. Kent DV, et al. (2003) A case for a comet impact trigger for the Paleocene/Eocene thermal maximum and carbon isotope excursion. *Earth Planet Sci Lett* 211(1–2):13–26.
12. Cramer BS, Kent DV (2005) Bolide summer: The Paleocene/Eocene thermal maximum as a response to an extraterrestrial trigger. *Palaeogeogr Palaeoclimatol Palaeoecol* 224(1–3):144–166.
13. Röhl U, Westerhold T, Bralower TJ, Zachos JC (2007) On the duration of the Paleocene–Eocene thermal maximum (PETM). *Geochem Geophys Geosyst* 8(12):1–13.
14. Cui Y, et al. (2011) Slow release of fossil carbon during the Palaeocene-Eocene thermal maximum. *Nat Geosci* 4(7):481–485.
15. Farley KA, Eltgroth SF (2003) An alternative age model for the Paleocene-Eocene thermal maximum using extraterrestrial 3He. *Earth Planet Sci Lett* 208(3–4):135–148.
16. Murphy BH, Farley KA, Zachos JC (2010) An extraterrestrial 3He-based timescale for the Paleocene-Eocene thermal maximum (PETM) from Walvis Ridge, IODP Site 1266. *Geochim Cosmochim Acta* 74(17):5098–5108.
17. Bains S, Corfield RM, Norris RD (1999) Mechanisms of climate warming at the end of the paleocene. *Science* 285(5428):724–727.
18. Müller RD, Sdrolias M, Gaina C, Steinberger B, Heine C (2008) Long-term sea-level fluctuations driven by ocean basin dynamics. *Science* 319(5868):1357–1362.
19. Harris AD, et al. (2010) Integrated stratigraphic studies of Paleocene–lowermost Eocene sequences, New Jersey Coastal Plain: Evidence for glacioeustatic control. *Paleoceanography* 25(3):PA3211.
20. Kopp RE, et al. (2009) An Appalachian Amazon? Magnetofossil evidence for the development of a tropical river-like system in the mid-Atlantic United States during the Paleocene-Eocene thermal maximum. *Paleoceanography* 24(4):PA4211.
21. Darton NH (1948) The Marlboro clay. *Econ Geol* 43(2):154–155.
22. Gibson T, Bybell L, Mason D (2000) Stratigraphic and climatic implications of clay mineral changes around the Paleocene/Eocene boundary of the northeastern US margin. *Sediment Geol* 134(1-2):65–92.
23. Self-Trail JM, Powars DS, Watkins DK, Wandless GA (2012) Calcareous nannofossil assemblage changes across the Paleocene-Eocene thermal maximum: Evidence from a shelf setting. *Mar Micropaleontol* 92-93:61–80.
24. Epstein S, Buchsbaum R, Lowenstam HA, Urey HC (1953) Revised carbonate-water isotopic temperature scale. *Geol Soc Am Bull* 64(11):1315–1326.
25. Kendall C, Coplen TB (2001) Distribution of oxygen-18 and deuterium in river waters across the United States. *Hydrol Processes* 15(7):1363–1393.
26. Chang G, et al. (2002) Nearshore physical processes and bio-optical properties in the New York Bight. *J. Geophys. Res* 107(C9):3133 (10.10292001).
27. Atkinson LP, Blanton J, Chandler W, Lee T (1983) Climatology of the southeastern United States continental shelf waters. *J Geophys Res* 88(C8):4705–4718.
28. Lentz SJ, Limeburner R (1995) The Amazon River Plume during AMASSEDS: Spatial characteristics and salinity variability. *J Geophys Res* 100(C2):2355–2375.
29. Van Houten FB (1962) Cyclic sedimentation and the origin of analcime-rich upper Triassic Lockatong Formation, west-central New Jersey and Adjacent Pennsylvania. *Am J Sci* 260:561–576.
30. Kahn A, Aubry MP (2004) Provincialism associated with the Paleocene/Eocene thermal maximum: Temporal constraint. *Mar Micropaleontol* 52(1):117–131.
31. Munk W, Dzieciuch M, Jayne S (2002) Millennial climate variability: Is there a tidal connection? *J Clim* 15(4):370–385.
32. Bond G, et al. (2001) Persistent solar influence on North Atlantic climate during the Holocene. *Science* 294(5549):2130–2136.
33. Keeling CD, Whorf TP (2000) The 1,800-year oceanic tidal cycle: A possible cause of rapid climate change. *Proc Natl Acad Sci USA* 97(8):3814–3819.
34. Sugarman PJ, Miller KG, Browning JV, et al. (2005) Millville Site. *Proceedings of the Ocean Drilling Program, Initial reports*, eds Miller KG, Sugarman PJ, Browning JV, et al. (Ocean Drilling Program, College Station, TX), Volume 174AX (Suppl.), 1–94.
35. Foukal P, Fröhlich C, Spruit H, Wigley TM (2006) Variations in solar luminosity and their effect on the Earth's climate. *Nature* 443(7108):161–166.
36. Reid GC (1991) Solar total irradiance variations and the global sea surface temperature record. *J Geophys Res* 96(D2):2835–2844.
37. Huybers P (2006) Early Pleistocene glacial cycles and the integrated summer insolation forcing. *Science* 313(5786):508–511.
38. Visbeck M, Chassignet EP, Curry RG, Delworth TL, Dickson RR, Krahmann G (2013) The ocean's response to North Atlantic oscillation variability, in The North Atlantic oscillation: Climatic significance and environmental impact, eds Hurrell JW, Kushnir Y, Ottersen G, Visbeck M, (American Geophysical Union, Washington, DC).
39. Levitus S, Boyer TP (1994) *World Ocean Atlas 1994. Volume 2. Oxygen.* (National Environmental Satellite, Data, and Information Service, Washington, DC).
40. Krantz DE, Kronick AT, Williams DF (1988) A model for interpreting continental-shelf hydrographic processes from the stable isotope and cadmium: Calcium profiles of scallop shells. *Palaeogeogr Palaeoclimatol Palaeoecol* 64(3–4):123–140.
41. Jones DS, Williams DF, Arthur MA (1983) Growth history and ecology of the Atlantic surf clam, Spisula solidissima (Dillwyn), as revealed by stable isotopes and annual shell increments. *J Exp Mar Biol Ecol* 73(3):225–242.
42. Schöne BR, et al. (2005) Climate records from a bivalved Methuselah (Arctica islandica, Mollusca; Iceland). *Palaeogeogr Palaeoclimatol Palaeoecol* 228(1):130–148.
43. Williams DF, Bé AW, Fairbanks RG (1981) Seasonal stable isotopic variations in living planktonic foraminifera from Bermuda plankton tows. *Palaeogeogr Palaeoclimatol Palaeoecol* 33(1):71–102.
44. Thunell R, Tappa E, Pride C, Kincaid E (1999) Sea-surface temperature anomalies associated with the 1997–1998 El Nino recorded in the oxygen isotope composition of planktonic foraminifera. *Geology* 27(9):843–846.
45. Kuehl SA, DeMaster DJ, Nittrouer CA (1986) Nature of sediment accumulation on the Amazon continental shelf. *Cont Shelf Res* 6(1–2):209–225.
46. DeMaster DJ, McKee BA, Nittrouer CA, Jiangchu Q, Guodong C (1985) Rates of sediment accumulation and particle reworking based on radiochemical measurements from continental shelf deposits in the East China Sea. *Cont Shelf Res* 4(1–2):143–158.
47. Nittrouer CA, et al. (1996) The geological record preserved by Amazon shelf sedimentation. *Cont Shelf Res* 16(5–6):817–841.
48. Broecker WS, Peng TH (1982) *Tracers in the Sea* (Eldigio Press Lamont Doherty Geological Observatory, Palisades, NY), p 690.
49. Siegenthaler U, Sarmiento JL (1993) Atmospheric carbon dioxide and the ocean. *Nature* 365(6442):119–125.
50. Revelle R, Suess HE (1957) Carbon dioxide exchange between atmosphere and ocean and the question of an increase of atmospheric CO2 during the past decades. *Tellus* 9(1):18–27.
51. Peng T-H, Key RM, Östlund HG (1998) Temporal variations of bomb radiocarbon inventory in the Pacific Ocean. *Mar Chem* 60(1):3–13.
52. Zeebe RE, Zachos JC (2013) Long-term legacy of massive carbon input to the Earth system: Anthropocene vs. Eocene. *Phil Trans R Soc A* 371(2001):20120006.
53. Caldeira K, Rampino MR (1990) Carbon dioxide emissions from Deccan volcanism and a K/T boundary greenhouse effect. *Geophys Res Lett* 17(9):1299–1302.
54. Dessert C, et al. (2001) Erosion of Deccan Traps determined by river geochemistry: Impact on the global climate and the Sr-87/Sr-86 ratio of seawater. *Earth Planet Sci Lett* 188(3–4):459–474.
55. Dickens GR, Castillo MM, Walker JCG (1997) A blast of gas in the latest Paleocene: Simulating first-order effects of massive dissociation of oceanic methane hydrate. *Geology* 25(3):259–262.
56. Schaller MF, Wright JD, Kent DV (2011) Atmospheric PCO_2 perturbations associated with the Central Atlantic Magmatic Province. *Science* 331(6023):1404–1409.
57. Schaller MF, Wright JD, Kent DV, Olsen PE (2012) Rapid emplacement of the Central Atlantic Magmatic Province as a net sink for CO2. *Earth Planet Sci Lett* 323–324(0): 27–39.
58. Archer D, et al. (2009) Atmospheric lifetime of fossil fuel carbon dioxide. *Annu Rev Earth Planet Sci* 37:117–134.
59. Stuiver M, Pearson GW, Braziunas TF (2006) Radiocarbon age calibration of marine samples back to 9000 cal yr BP. *Radiocarbon* 28(2B):980–1021.
60. Bowen GJ, Bowen BB (2008) Mechanisms of PETM global change constrained by a new record from central Utah. *Geology* 36(5):379–382.
61. Sluijs A, et al. (2007) Environmental precursors to rapid light carbon injection at the Palaeocene/Eocene boundary. *Nature* 450(7173):1218–1221.
62. Zachos JC, et al. (2006) Extreme warming of mid-latitude coastal ocean during the Paleocene-Eocene thermal maximum: Inferences from TEX86 and isotope data. *Geology* 34(9):737–740.
63. Stassen P, Thomas E, Speijer RP (2012) Integrated stratigraphy of the Paleocene-Eocene thermal maximum in the New Jersey Coastal Plain: Toward understanding the effects of global warming in a shelf environment. *Paleoceanography* 27(4): PA4210.
64. Nunes F, Norris RD (2006) Abrupt reversal in ocean overturning during the Palaeocene/Eocene warm period. *Nature* 439(7072):60–63.
65. Nicolo MJ, Dickens GR, Hollis CJ (2010) South Pacific intermediate water oxygen depletion at the onset of the Paleocene-Eocene thermal maximum as depicted in New Zealand margin sections. *Paleoceanography* 25(4):PA4210.
66. Mollenhauer G, et al. (2005) An evaluation of 14C age relationships between cooccurring foraminifera, alkenones, and total organic carbon in continental margin sediments. *Paleoceanography* 20(1):PA1016.
67. Schneider-Mor A, Bowen GJ (2013) Coupled and decoupled responses of continental and marine organic-sedimentary systems through the Paleocene-Eocene thermal maximum, New Jersey margin. *Paleoceanography* 28:105–115.
68. Panchuk K, Ridgwell A, Kump L (2008) Sedimentary response to Paleocene-Eocene thermal maximum carbon release: A model-data comparison. *Geology* 36(4):315–318.
69. Zeebe RE, Zachos JC, Dickens GR (2009) Carbon dioxide forcing alone insufficient to explain Palaeocene-Eocene thermal maximum warming. *Nat Geosci* 2(8):576–580.
70. Hönisch B, et al. (2012) The geological record of ocean acidification. *Science* 335(6072): 1058–1063.
71. Wang H, Kent DV, Jackson MJ (2013) Evidence for abundant isolated magnetic nanoparticles at the Paleocene-Eocene boundary. *Proc Natl Acad Sci USA* 110(2): 425–430.